catalysts

MDPI

Article

Kinetic Modeling of the Direct Dimethyl Ether (DME) Synthesis over Hybrid Multi-Site Catalysts

Antonio D'Ambrosio [1], Alice Bertino [1], Serena Todaro [2], Mariarita Santoro [2], Catia Cannilla [2], Francesco Frusteri [2], Giuseppe Bonura [2,*], Leone Mazzeo [1,*] and Vincenzo Piemonte [1]

[1] Unit of Chemical-Physics Fundamentals in Chemical Engineering, Faculty of Science and Technology for Sustainable Development and One Health, University Campus Bio-Medico of Rome, Via Alvaro del Portillo 21, 00128 Rome, Italy; antonio.dambrosio@unicampus.it (A.D.); alice.bertino@unicampus.it (A.B.); v.piemonte@unicampus.it (V.P.)

[2] CNR-ITAE, Istituto di Tecnologie Avanzate per l'Energia "Nicola Giordano", Via S. Lucia sopra Contesse 5, 98126 Messina, Italy; serena.todaro@cnr.it (S.T.); mariarita.santoro@cnr.it (M.S.); catia.cannilla@cnr.it (C.C.); francesco.frusteri@cnr.it (F.F.)

* Correspondence: giuseppe.bonura@cnr.it (G.B.); l.mazzeo@unicampus.it (L.M.)

Abstract: This paper deals with the proposition of a kinetic model for the direct synthesis of DME via CO_2 hydrogenation in view of the necessary optimization of the catalytic system, reactor design, and process strategy. Despite the fact that DME synthesis is typically treated as a mere combination of two separated catalytic steps (i.e., methanol synthesis and methanol dehydration), the model analysis is now proposed by taking into account the improvements related to the process running over a hybrid catalyst in a rational integration of the two catalytic steps, with boundary conditions properly assumed from the thermodynamics of direct DME synthesis. Specifically, the CO_2 activation step at the metal–oxide interface in the presence of ZrO_2 has been described for the first time through the introduction of an ad hoc mechanism based on solid assumptions from inherent studies in the literature. The kinetic modeling was investigated in a tubular fixed-bed reactor operating from 200 to 260 °C between 1 and 50 bar as a function of a gas hourly space velocity ranging from 2500 to 60,000 NL/kg_{cat}/h, in a stoichiometric CO_2/H_2 feed mixture of 1:3 v/v. A well-detailed elementary mechanism was used to predict the CO_2 conversion rate and identify the key reaction pathways, starting with the analysis of the implicated reactions and corresponding kinetic mechanisms and expressions, and finally estimating the main parameters based on an appropriate modeling of test conditions.

Keywords: dimethyl ether; CO_2 valorization; hydrogen conversion; hybrid catalysts; kinetic modeling; fixed-bed reactor

Citation: D'Ambrosio, A.; Bertino, A.; Todaro, S.; Santoro, M.; Cannilla, C.; Frusteri, F.; Bonura, G.; Mazzeo, L.; Piemonte, V. Kinetic Modeling of the Direct Dimethyl Ether (DME) Synthesis over Hybrid Multi-Site Catalysts. *Catalysts* **2024**, *14*, 61. https://doi.org/10.3390/catal14010061

Academic Editors: Enrico Catizzone and Ana Palčić

Received: 20 December 2023
Revised: 4 January 2024
Accepted: 11 January 2024
Published: 13 January 2024

1. Introduction

In consideration of the growing concern for climate change, the search for novel development models based on renewable energy sources with the potential to gradually replace fossil fuels is in the spotlight. On this road to progressive decarbonization, dimethyl ether (DME), the simplest of the ether compounds (chemical formula CH_3OCH_3), has been recently proposed as a very promising alternative fuel [1–3], being characterized by its high cetane number, low auto-ignition temperature, and near-zero emissions of particulate matter, carbon monoxide, and unburned hydrocarbons [4,5]. It also presents chemical and physical properties similar to LPG, enabling the use of existing storage and distribution infrastructure [6]. Additionally, DME can serve as a feedstock for the production of olefins via the DTO (DME-to-olefins) reaction pathway, which is characterized by high yields and conversions [7–9].

However, the real appeal of this compound lies in its potential synthesis reaction (Equation (1)), since recent research frontiers aim to employ CO_2 and H_2 as reactants [10,11]:

$$2CO_2 + 6H_2 \rightleftharpoons CH_3OCH_3 + 3H_2O\left(\Delta H^0 = -122\ \text{kJ/mol}\right) \quad (1)$$

Using captured CO_2 and green H_2 produced via electrolysis, it is, therefore, possible to configure DME as an e-fuel directly produced in a sustainable CCUS (carbon capture utilization and storage) technology chain [12,13]. Furthermore, even though this aspect is still under investigation, DME can be steam-reformed, making it a potential circular hydrogen carrier [14]. For this to be feasible, however, it is necessary to make the synthesis process more efficient and cost-effective. Currently, DME is primarily produced from synthesis gas through an indirect method involving the use of two reactors in a typical cascade process [15]. In the first reactor, methanol synthesis is performed on a ternary metal–oxide catalyst (typically CZA, which is CuO-ZnO-Al_2O_3), while the second reactor allows the dehydration of the previously formed methanol over an acidic catalytic bed (usually γ-Al_2O_3 or a zeolite sample, such as HZSM-5) [10,16–18]. The real challenge is to achieve effective process intensification by implementing direct synthesis in a single reactor, using CO_2 as a feedstock, thus allowing the valorization of a thermodynamically "inert" compound, as well as reducing operating and investment costs [19,20]. Certainly, the main concern is the development of a multi-functional catalyst wherein a long-range inter-dispersion among metallic, oxide, and acidic functionalities must be achieved to catalyze both the methanol synthesis and DME production steps [14,21]. Indeed, by hybridizing the catalytic system for direct DME synthesis, the thermodynamic limitations behind the CO_2 hydrogenation process stopping the formation of methanol can be overcome, even if unavoidable water generation is a key contributor to possible catalyst deactivation mechanisms, such as copper sintering or migration of weak acidic sites [22–24].

Given the potential and critical issues associated with the direct synthesis of dimethyl ether from hydrogen and carbon dioxide, this work aims at investigating the performance, on a laboratory scale, of a previously optimized hybrid CuO-ZnO-ZrO_2/HZSM-5 catalytic system [22] by developing a kinetic model suitable to predict its experimental behavior in a wide set of operating conditions. Particularly, the exchange of alumina (a key component in the benchmark catalyst for methanol synthesis) with zirconia to enhance CO_2 adsorption, water tolerance, and heat management [25] has been limitedly studied from a microkinetic point of view [26,27]. Therefore, this knowledge gap inspired an ad hoc 18-parameter model based on three cascade steps (i.e., CO_2 hydrogenation to methanol, methanol dehydration, and rWGS) occurring in one pot over a hybrid catalytic system. This model aims at explaining a dual-site mechanism on two different adsorption sites by claiming that the CO_2 activation step at the metal–oxide interface is crucial prior to undergoing hydrogenation to methanol. Acidic functionality is then necessary for the subsequent dehydration into DME. As a consequence, the corresponding kinetic expressions were derived and appropriately integrated with all the reactions involved in the process. This resulted in a comprehensive model for the direct synthesis of DME, which led to the assessment of new mechanistic clues about the activity–selectivity pattern of the catalyst under investigation as necessary for further optimization of its design.

2. Experimental Section

This section is divided into two parts: synthesis of the hybrid catalyst and validation of its performance through a fixed-bed reactor.

2.1. Catalyst Synthesis

The hybrid catalyst was synthesized through the gel oxalate coprecipitation method, as elsewhere described [28]. Firstly, the nitrate precursors, namely $Cu(NO_3)_2{\cdot}2.5H_2O$, $Zn(NO_3)_2{\cdot}6H_2O$, and $ZrO(NO_3)_2{\cdot}nH_2O$ (in a relative Cu/Zn/Zr atomic ratio of 60/30/10), were dissolved in an ethanolic solution and added, at room temperature in a slow and

constant mode, to a vigorously stirred ethanolic solution containing oxalic acid (20 wt.% in excess with respect to the stoichiometric amount necessary to precipitate the metal precursors) and the finely dispersed HZSM-5 zeolite (Si/Al = 23 mol/mol) in a weight ratio of 1:1 with respect to the final oxide composition of the catalyst. The precipitate was stirred for 3 h, then aged overnight. The catalyst was filtered, dried at 90 °C for 16 h, and then calcined at 350 °C for 4 h.

2.2. Catalyst Testing

In order to assess the activity of the hybrid catalyst, CO_2 hydrogenation to DME was studied in a full kinetic regime, according to conditions designed to rule out the control of diffusional phenomena [11,17]. All the catalytic measurements were carried out in a fixed-bed stainless steel reactor with an internal diameter of 4 mm and a length of 21 mm, loaded with 250 mg of catalyst, and housed within a stainless-steel rod to minimize temperature gradients. The 40–70 mesh (210–420 μm) fraction was selected as a suitable compromise between reactor pressure drop and catalyst particle mechanical resistance. Catalytic tests were carried out at a total pressure of 1, 10, 30, or 50 bar in a temperature range between 200 and 260 °C and gas hourly space velocity of 2500, 8800, and 60,000 NL/kg_{cat}/h, employing a feed mixture of $CO_2/H_2/N_2$ in a 3:9:1 v/v ratio. Before each test, the catalyst underwent an in situ reduction at 300 °C for 1 h using pure hydrogen flow at atmospheric pressure. The reaction stream was analyzed via a gas chromatograph equipped with a three-column separation system connected to a flame ionization detector (FID) and a thermal conductivity detector (TCD). No formation of methane or higher hydrocarbons was detected under the applied conditions. Quantitative data were expressed in terms of CO_2 conversion (X_{CO_2}), DME yield (Y_{DME}) and DME and CO selectivity (S_{DME} and S_{CO}), as defined in Equations (2)–(5):

$$X_{CO_2} = \frac{F^{in}_{CO_2} - F^{out}_{CO_2}}{F^{in}_{CO_2}} \quad (2)$$

$$Y_{DME} = \frac{F^{out}_{DME}}{F^{in}_{CO_2}} \quad (3)$$

$$S_{DME} = \frac{F^{out}_{DME}}{F^{out}_{DME} + F^{out}_{Meth} + F^{out}_{CO}} \quad (4)$$

$$S_{CO} = \frac{F^{out}_{CO}}{F^{out}_{DME} + F^{out}_{Meth} + F^{out}_{CO}} \quad (5)$$

In Equations (2)–(5), F^{in}_i and F^{out}_i are the inlet and the outlet molar flow rates of component i, respectively. Conversion and selectivity data were determined by both internal standard and mass-balance methods, averaging three independent measurements with an accuracy of ±3%.

3. Kinetic Modeling

The development of a kinetic model for direct CO_2-to-DME hydrogenation was carried out in two steps:

1. Analysis of the implicated reactions and corresponding kinetic mechanisms and expressions.
2. Estimation of missing parameters based on appropriate modeling of test conditions.

3.1. Reaction Kinetics Investigation

In direct DME synthesis from CO_2 and H_2, three reactions (Equations (6)–(8)) are involved [10,29–31]:

1. CO_2 hydrogenation to methanol (CHM):

$$CO_2 + 3H_2 \rightleftharpoons CH_3OH + H_2O \left(\Delta H^0 = -49\ \text{kJ/mol}\right) \quad (6)$$

2. Methanol dehydration to DME (MDD):

$$2CH_3OH \rightleftharpoons CH_3OCH_3 + H_2O \left(\Delta H^0 = -23\ \text{kJ/mol}\right) \quad (7)$$

3. Reverse water–gas shift (rWGS):

$$CO_2 + H_2 \rightleftharpoons CO + H_2O \left(\Delta H^0 = +41\ \text{kJ/mol}\right) \quad (8)$$

CO hydrogenation to DME is not considered since it can be obtained from the linear combination of Equations (7) and (8), and is also significantly inhibited by the production of formate, an intermediate that strongly binds copper active sites [32,33]. For each reaction, the kinetic mechanism was reconstructed, identifying the rate-determining step (r.d.s.) [34]. As for methanol dehydration and rWGS, previously elaborated mechanisms from the literature were adopted due to the conventional nature of the employed catalyst (HZSM-5 and Cu-based systems, respectively) [35,36], while an ad hoc kinetic mechanism was developed for CO_2 hydrogenation, based on experimental evidence [37]. Finally, the kinetic expression of the reaction rate was derived for each mechanism, assuming that all elementary steps, except the r.d.s., were at thermodynamic equilibrium and adopting the Langmuir–Hinshelwood–Hougen–Watson (LHHW) model [38]. In light of the moderate operating conditions in terms of pressure and temperature, the gas phase was assumed to be ideal, with a unitary fugacity coefficient (see Appendix A). A "dual site" model is thus proposed, distinguishing two different active sites on the hybrid catalyst [37,39]: the metal–oxide site (σ) and the zeolitic acid site $\left(\widetilde{\sigma}\right)$.

3.1.1. CO_2 Hydrogenation Mechanism

The introduction of zirconia in the catalyst composition, instead of the alumina present in the benchmark catalyst, has a limited history in the literature related to kinetic modeling [26]. Thus, an ad hoc mechanism was developed to further explore its specific behavior. More in detail, the CO_2 activation step is a highly debated aspect, with two generally proposed alternatives [40,41]: the formate route, based on the formation of HCOO intermediate, and the rWGS route, which involves the conversion of CO_2 into CO. Although an unambiguous agreement on the exact mechanism does not exist yet, most of the recent experimental findings suggest a leaning towards the formate route, as described by Equations (9a)–(9j):

$$(3x)\ H_2 + 2\sigma \rightleftharpoons 2H\sigma \quad (9a)$$

$$CO_2 + \sigma \rightleftharpoons CO_2\sigma \quad (9b)$$

$$CO_2\sigma + H\sigma \rightleftharpoons CHO_2\sigma + \sigma\ r.d.s. \quad (9c)$$

$$CHO_2\sigma + H\sigma \rightleftharpoons CH_2O_2\sigma + \sigma \quad (9d)$$

$$CH_2O_2\sigma + H\sigma \rightleftharpoons CH_2O(OH)\sigma + \sigma \quad (9e)$$

$$CH_2O(OH)\sigma + H\sigma \rightleftharpoons CH_2O\sigma + H_2O\sigma \quad (9f)$$

$$H_2O\sigma \rightleftharpoons H_2O + \sigma \quad (9g)$$

$$CH_2O\sigma + H\sigma \rightleftharpoons CH_3O\sigma + \sigma \quad (9h)$$

$$CH_3O\sigma + H\sigma \rightleftharpoons CH_3OH\sigma + \sigma \quad (9i)$$

$$CH_3OH\sigma \rightleftharpoons CH_3OH + \sigma \quad (9j)$$

According to this route, one molecule of CO_2 activated on a partially oxidized Cu(δ+) site (9b) initially reacts with one atom of hydrogen previously activated on a metallic site (9a), giving rise to a formate species (9c). The latter then reacts with other activated hydrogen atoms in a cascade sequence to produce dioxomethylene species (9d), formaldehyde (9f), methoxy species (9f), and finally methanol (9i) in the last hydrogenation step.

3.1.2. Methanol Dehydration Mechanism

The methanol dehydration reaction strongly relies on the zeolitic component of the catalyst, considering that density, strength, accessibility, and nature of the acid sites (Brønsted or Lewis) are all features capable of influencing the DME productivity [22,37,42]. Several kinetic models have been proposed in the literature, primarily differing from the zeolite topology [26]. However, in terms of reaction mechanism, most studies have converged on identifying two main alternative pathways [42,43]:

Associative pathway, which involves the formation of DME from two adsorbed methanol molecules.

The dpathway is characterized by the adsorption of a methanol molecule followed by its dissociation into a methoxyl group, which then reacts with another methanol molecule to produce DME.

Overall, due to the relatively low operating temperatures (far below 400 °C) and the mesoporous structure of the hybrid catalyst utilized [25], it can be concluded that the predominant pathway is the associative one [44]. Concerning the mechanism over a HZSM-5 zeolite, Lu et al. [35] proposed the following sequence of elementary reactions (Equations (10a)–(10d)):

$$(2x)\ CH_3OH + \widetilde{\sigma} \rightleftharpoons CH_3OH\widetilde{\sigma} \quad (10a)$$

$$CH_3OH\widetilde{\sigma} \rightleftharpoons CH_2\widetilde{\sigma} + H_2O \quad (10b)$$

$$CH_2\widetilde{\sigma} + CH_3OH\widetilde{\sigma} \rightleftharpoons CH_3OCH_3\widetilde{\sigma} + \widetilde{\sigma}\ r.d.s. \quad (10c)$$

$$CH_3OCH_3\widetilde{\sigma} \rightleftharpoons CH_3OCH_3 + \widetilde{\sigma} \quad (10d)$$

3.1.3. rWGS Mechanism

The rWGS reaction mechanism can be reconstructed based on its counterpart reaction. More specifically, WGS predominantly occurs on copper sites (at the interface with other metal oxides), meaning that the introduction of zirconia can act as a promoter, enhancing the activity of the existing sites without inducing any further reaction [45,46]. It is therefore possible to refer to some mechanisms already found in the literature that identify the carboxyl route as the predominant pathway for the WGS reaction [36,47], as exemplified by the set of Equations (11a)–(11g):

$$H_2O + \sigma \rightleftharpoons H_2O\sigma \quad (11a)$$

$$H_2O\sigma + \sigma \rightleftharpoons OH\sigma + H\sigma\ r.d.s. \quad (11b)$$

$$CO + \sigma \rightleftharpoons CO\sigma \quad (11c)$$

$$CO\sigma + OH\sigma \rightleftharpoons COOH\sigma + \sigma \quad (11d)$$

$$COOH\sigma + \sigma \rightleftharpoons CO_2\sigma + H\sigma \quad (11e)$$

$$2H\sigma \rightleftharpoons H_2 + 2\sigma \quad (11f)$$

$$CO_2\sigma \rightleftharpoons CO_2 + \sigma \quad (11g)$$

3.2. Dual-Site Adsorption on the Hybrid Catalyst

While the final dehydration step of methanol to DME is known to be mediated by the zeolitic acidic site [15,16,18], an adequate concentration of both metallic and metal–oxide sites is claimed to be somehow necessary for the primary methanol formation [32,33]. In

particular, it should be noted that the adsorption of CO_2 can even occur on bare oxides, while the dissociation of H_2 more efficiently takes place on metallic surfaces; however, a possible activation over metal–oxide surfaces is not ruled out [40,41]. Therefore, this model proposes the use of a unique metal–oxide site for both CO_2 and H_2 adsorption, assumed to be the active center in CO_2 hydrogenation to methanol and in rWGS reaction. Accordingly, the rate equations proposed for this dual-site LHHW mechanism are summarized in Equations (12)–(14):

$$r_{CHM} = \frac{K_{cin_{CHM}}\left(P_{CO_2}P_{H_2}^{1/2} - \frac{P_{CH_3OH}P_{H_2O}}{K_{eq_{CHM}}P_{H_2}^{5/2}}\right)}{\left(1 + K_{CO}P_{CO} + K_{CO_2}P_{CO_2} + K_{CH_3OH}P_{CH_3OH} + K_{H_2O}P_{H_2O} + \sqrt{K_{H_2}P_{H_2}}\right)^2} \quad (12)$$

$$r_{MDD} = \frac{K_{cin_{MDD}}\left(P_{CH_3OH}^2 - \frac{P_{CH_3OCH_3}P_{H_2O}}{K_{eq_{MDD}}}\right)}{\left(1 + K_{H_2O}P_{H_2O} + K_{CH_3OH}P_{CH_3OH} + K_{CH_3OCH_3}P_{CH_3OCH_3}\right)^2} \quad (13)$$

$$r_{rWGS} = -\frac{K_{cin_{rWGS}}\left(P_{H_2O}P_{CO} - \frac{P_{CO_2}P_{H_2}}{K_{eq_{rWGS}}}\right)}{\left(1 + K_{CO}P_{CO} + K_{CO_2}P_{CO_2} + K_{CH_3OH}P_{CH_3OH} + K_{H_2O}P_{H_2O} + \sqrt{K_{H_2}P_{H_2}}\right)^2} \quad (14)$$

Remarkably, since both the steps of CO_2 hydrogenation to methanol and rWGS are characterized by a competition for the same adsorption site (σ), the denominators of Equations (12) and (14) include the terms for CO adsorption ($K_{CO}P_{CO}$) and CH_3OH adsorption ($K_{CH_3OH}P_{CH_3OH}$), respectively, as inhibition contributions for the corresponding reactions.

3.3. Parameter Estimation Method

In order to validate the kinetic expressions, it is necessary to describe the laboratory setup via a predictive model, which is crucial for parameter estimation. In this light, the fixed-bed reactor was assimilated to an isothermal and isobaric PFR (plug flow reactor). The experimental setup was designed to minimize the impact of internal and external diffusional resistances, which were consequently neglected. Therefore, one-dimensional steady-state mass balances (Equations (15) and (16)) were written for each compound along the axial coordinate:

$$\frac{dG_i}{dz} = \frac{1}{L}\sum_{j=1}^{3}\nu_{ij}r_j \quad (15)$$

$$G_i(z=0) = y_i^{in}G_{TOT}^{in} \quad (16)$$

In Equation (15), L represents the reactor length, r_j is the rate of reaction j (Equations (12)–(14)) and ν_{ij} is the stoichiometric coefficient of compound i in reaction j. In Equation (16), y_i^{in} is the inlet molar fraction of component i and G_{TOT}^{in} is the total inlet gas hourly space velocity. The balances are, indeed, expressed in terms of space velocity of each compound, noted as G_i, which is here defined as the ratio between the molar flow rate F_i and the total weight of the catalyst M_c (Equation (17)):

$$G_i = \frac{F_i}{M_c} \quad (17)$$

It is important to note that the kinetic expressions of reaction rates (present in Equation (15)) incorporate temperature-dependent equilibrium, kinetic, and adsorption constants. While the former can be derived from the existing literature, being only subject to the thermodynamics of the reactions involved (see Table 1) [48], the latter two constants are specific to the developed catalyst and require experimental data regression for determination. More precisely, the Arrhenius and Van 't Hoff equations express their temperature

dependence and were reparametrized (see Equations (18) and (19)) to improve numerical stability in fitting and decrease numerical correlation between estimated parameters [49,50]:

$$K_{cin_j} = k_{cin_j} exp\left[-E_{A_j}\left(\frac{T_{rif}}{T_R} - 1\right)\right] \tag{18}$$

$$K_i = k_i exp\left[-\Delta H_{ads_i}\left(\frac{T_{rif}}{T_R} - 1\right)\right] \tag{19}$$

Table 1. Expressions of equilibrium constants' dependence on temperature [48].

Parameter	Temperature Dependence
$K_{eq_{CHM}}$	$10^{\frac{3066}{T} - 10.592} \quad [bar^{-2}]$
$K_{eq_{MDD}}$	$\exp\left(\frac{4019}{T} + 3.707 \cdot log(T) - 2.783 \cdot 10^{-3} \cdot T + +3.8 \cdot 10^{-7} \cdot T^2 - 6.561 \cdot 10^4 \cdot T^{-3} - 26.64\right)$
$K_{eq_{rWGS}}$	$10^{-\frac{2073}{T} + 2.029}$

In Equations (18) and (19), T_{rif} is a reference temperature, assumed to be equal to the experimental mean value of 503.15 K; T_R denotes the reactor temperature; k_{cin_j} and k_i are pre-exponential factors; and E_{A_j} and ΔH_{ads_i} represent energetic terms. The latter were made dimensionless, according to Equations (20) and (21) (where R is the universal gas constant), to decrease differences in magnitude orders and reduce computational costs [51]:

$$E_{A_j} = \frac{E^*_{A_j}}{T_{rif} R} \tag{20}$$

$$\Delta H_{ads_i} = \frac{\Delta H^*_{ads_i}}{T_{rif} R} \tag{21}$$

Both pre-exponential factor and energetic terms were estimated by minimizing the weighted sum ϕ of square relative errors between experimental molar fractions Y_i^k and model outputs $\hat{Y}_i^k$ (Equation (22)) [52]:

$$\phi = \sum_{k=1}^{N_p} \sum_i \left[w_i \cdot \left(\frac{Y_i^k - \hat{Y}_i^k}{Y_i^k} \right)^2 \right] \tag{22}$$

In Equation (22), N_p represents the number of experimental tests, while w_i is the weight assigned to compound i. Optimization was carried out by applying a Matlab algorithm based on the *fmincon* function to find the minimum value, providing a set of 100 experimental data points as input. The starting point was varied in different trials, looking at achieving a global minimum, while an additional set of 60 data points was used to validate the outcomes obtained.

4. Results and Discussion

4.1. Experimental Results

A sensitivity analysis was carried out to evaluate the influence of temperature and pressure on product distribution, as depicted in Figure 1.

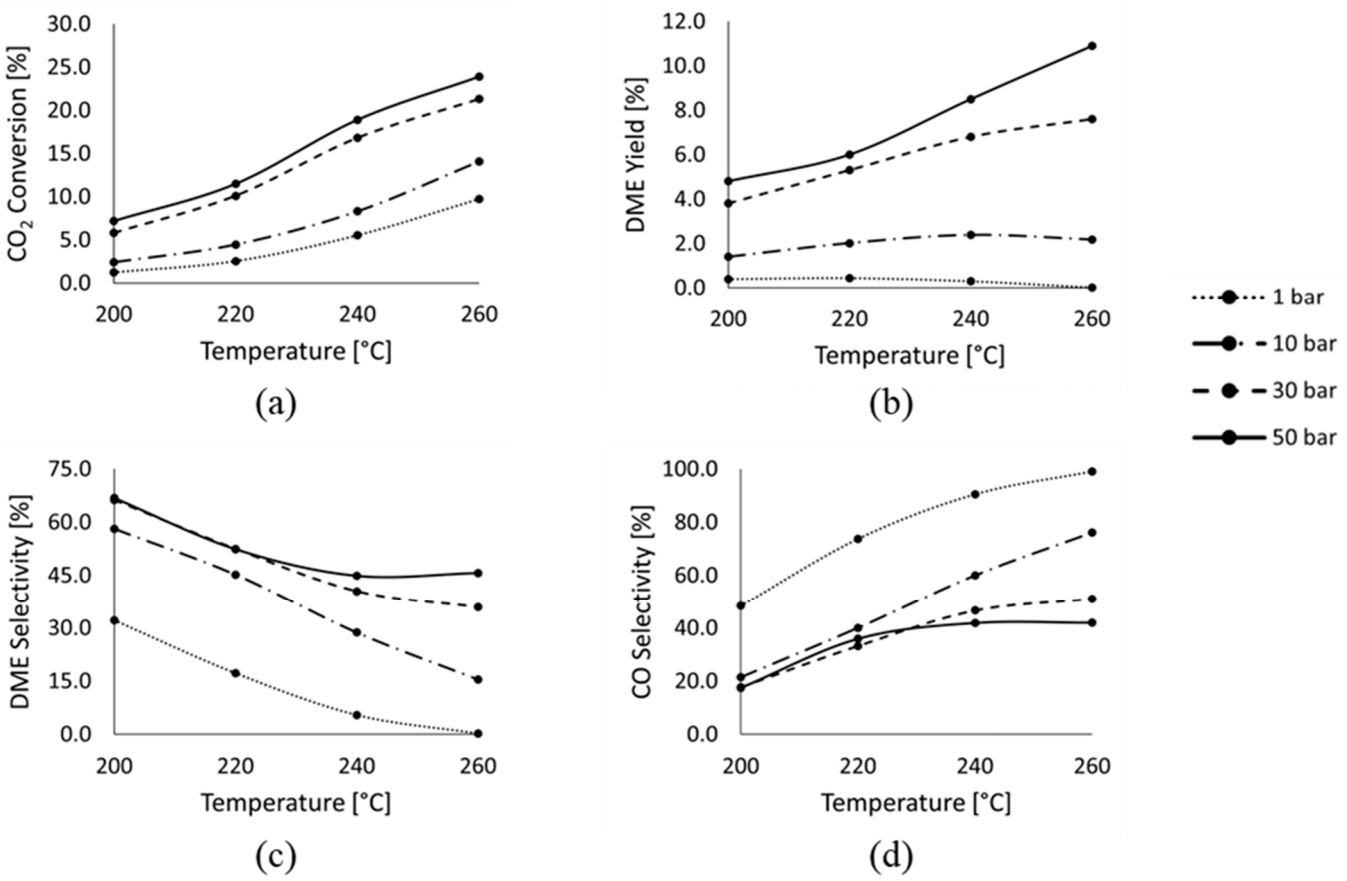

Figure 1. Influence of temperature and pressure on CO_2 conversion (**a**), DME yield (**b**), DME selectivity (**c**), and CO selectivity (**d**), evaluated with an inlet flow rate of 8800 NL/(kg_{cat} h).

On the whole, the results are consistent with the thermodynamic analysis of the system [10,31,53]. High pressure is preferable during the DME synthesis reaction as it leads to a decrease in the number of moles. On the other hand, an increase in temperature favors CO_2 conversion due to its positive kinetic effect on the reaction rate. However, it simultaneously decreases DME selectivity while raising CO selectivity, in agreement with the thermal tonality both of DME synthesis (exo-) and rWGS (endo-). Although a plateau in DME and CO selectivity was observed above 240 °C for runs performed both at 30 and 50 bar, a further increase in reaction temperature unfortunately triggers severe catalyst deactivation. Indeed, a larger amount of water formed above those conditions dramatically determines morphological changes in the catalyst surface, prompting a drastic activity decay (ca. 20% with respect to the initial activity) in a few hours of time on stream (<20 h) [17,22]. Therefore, these findings not only indicate that the process performance is governed by kinetics [15], but also suggest an optimal compromise between CO_2 conversion and DME selectivity at moderately high pressures (30 or 50 bar) and intermediate temperatures (<260 °C), so as to limit any issue related to catalyst lifetime.

4.2. Reaction Kinetics Investigation Results

Falling within the typical range of values reported for similar computational models [26], the parameters resulting from the estimation procedure are listed in Table 2, with Figure 2 illustrating the comparison between experimental data and model outputs.

Table 2. Estimated parameters for the proposed kinetic model and corresponding confidence interval with a level of significance equal to 0.05.

Parameter	Unit	Pre-Exponential Factor (k_{cin_j} or k_i)	Energetic Term (E_{A_j} or $-\Delta H_{ads_i}$)
$K_{cin_{CHM}}$	$\left[mol \cdot g_{cat}^{-1} \cdot s^{-1} \cdot bar^{-3/2}\right]$	$(2.56 \pm 0.05) \cdot 10^{-4}$	44.95 ± 1.75
$K_{cin_{MDD}}$	$\left[mol \cdot g_{cat}^{-1} \cdot s^{-1} \cdot bar^{-2}\right]$	0.26 ± 0.01	99.73 ± 1.21
$K_{cin_{rWGS}}$	$\left[mol \cdot g_{cat}^{-1} \cdot s^{-1} \cdot bar^{-2}\right]$	$(6.16 \pm 0.12) \cdot 10^{-3}$	39.52 ± 1.71
K_{H_2}	$\left[bar^{-1}\right]$	$(8.54 \pm 0.32) \cdot 10^{-2}$	33.57 ± 1.38
K_{CO_2}	$\left[bar^{-1}\right]$	9.56 ± 0.10	14.23 ± 0.93
K_{CO}	$\left[bar^{-1}\right]$	8.97 ± 0.49	10.41 ± 0.40
K_{H_2O}	$\left[bar^{-1}\right]$	8.02 ± 0.43	22.95 ± 0.86
K_{CH_3OH}	$\left[bar^{-1}\right]$	5.70 ± 0.29	7.07 ± 0.11
$K_{CH_3OCH_3}$	$\left[bar^{-1}\right]$	5.20 ± 0.10	60.53 ± 0.66

The model provided satisfactory results in calculating the molar fractions of CO_2 and H_2, with an average relative error of 1.5%, which is comparable to the chromatographic tolerance. Moreover, despite an average relative error of around 40%, the model suitably also works in the prediction of the molar fractions of DME and CO, considering a minimal absolute error in the order of 0.001. Only in the case of the other compounds (i.e., CH_3OH or H_2O), the large number of estimated parameters (which is equal to 18) cannot determine a lower discrepancy in the model fitting, so that a relatively small error in absolute terms has a strong impact in relative terms.

In any case, even the highest deviation recorded for large methanol concentrations (see Figure 2f) cannot be considered a relevant issue since the simulation model targets the one-pot synthesis of DME and the methanol selectivity always attains relatively low values (below 10%) under all the experimental conditions applied. More importantly, these results evidently confirmed previous mechanistic clues on the catalytic behavior, with positive effects on the process performance played by an increase in space velocity or reaction pressure. However, further optimization of the hybrid catalyst design is required for higher CO_2 conversion rates below 220 °C, where CO formation can be minimized. Finally, not only the catalyst formulation but also the reactor configuration should be properly designed in order to tackle the issues related to water formed during the process, dramatically affecting catalyst lifetime and process performance.

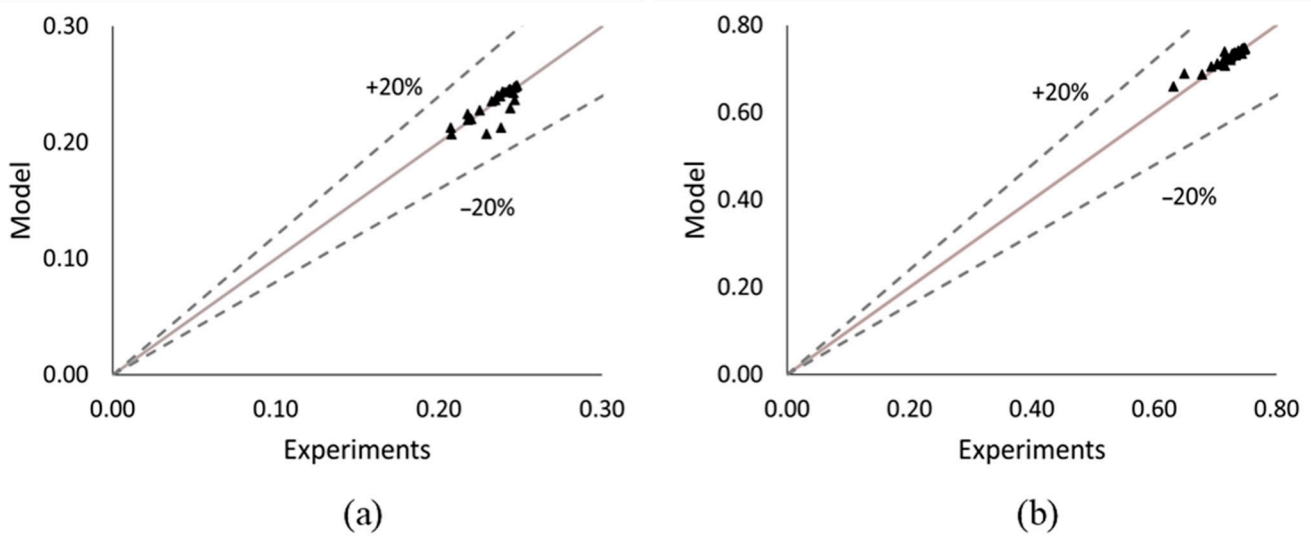

Figure 2. *Cont.*

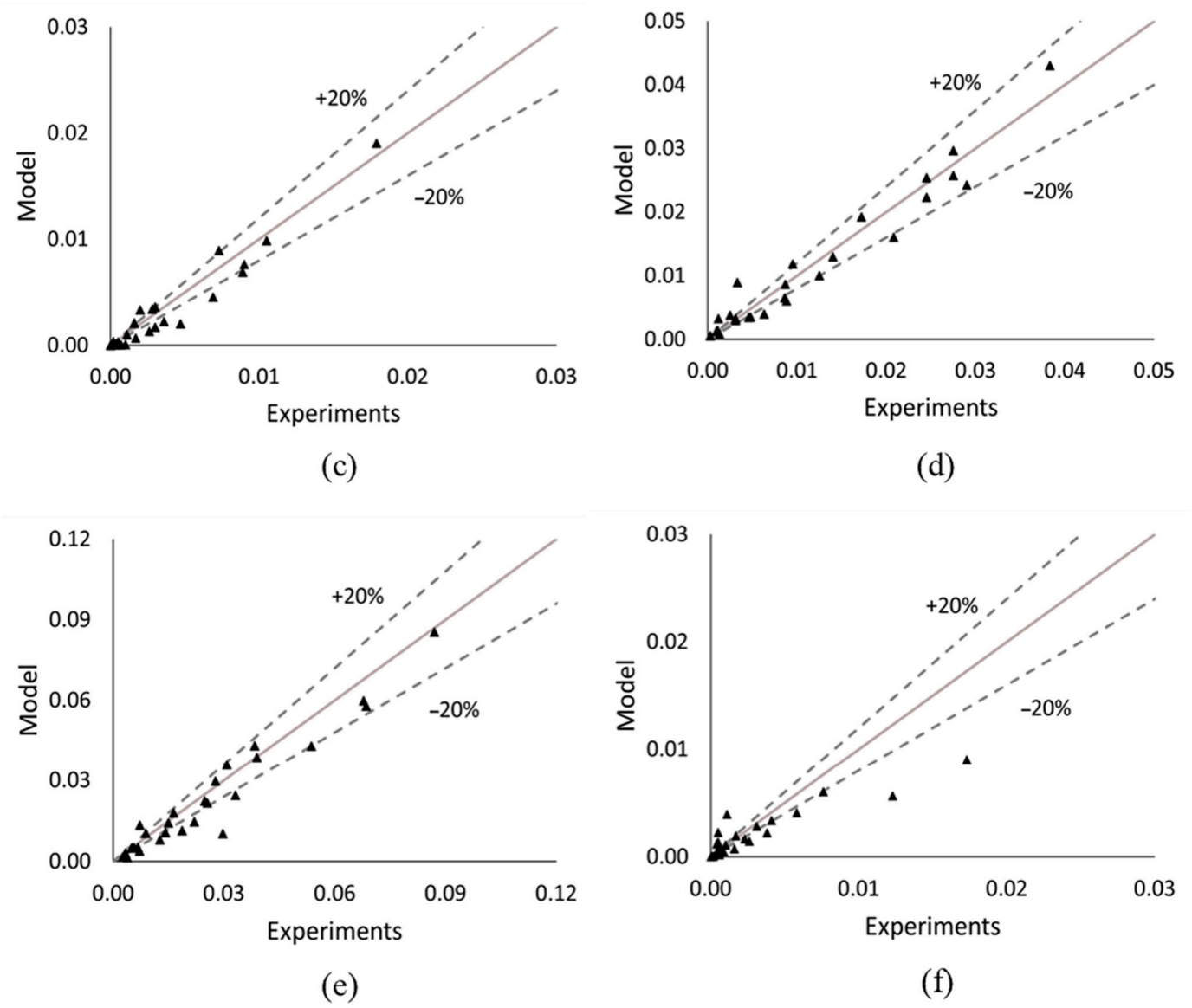

Figure 2. Comparison of experimental data (along the x-axis) and model results (along the y-axis) for the mole fractions of CO_2 (**a**), H_2 (**b**), DME (**c**), CO (**d**), H_2O (**e**), and methanol (**f**).

5. Conclusions

A comprehensive 18-parameter kinetic model was developed for the direct hydrogenation of CO_2 to DME over a hybrid CuO-ZnO-ZrO_2/HZSM-5 catalytic system, previously optimized in terms of composition, preparation method, and tuning of physico-chemical properties. The model was validated in a wide set of reaction pressure, temperature, and space velocity, clearly showing a reliable fitting of the estimated parameters, within an average absolute error of 10^{-4}, both for the process reactants (i.e., CO_2, H_2) and the target product (i.e., DME), with the correspondent experimental values. The accuracy of the model confirmed previous findings on the multi-site nature of the studied process, mainly following the formate route, according to which carbon dioxide is activated at the metal–oxide interface, then reacting with activated hydrogen migrating via spillover from metallic copper sites. Afterwards, formate species are hydrogenated to methanol, which, in line with an associative pathway, quickly turns into DME by condensation with another adsorbed methanol molecule over the acidic sites of the zeolite. Overall, the adequate accuracy in the prediction of the compositions related to the most abundant process compounds makes the model promising for further implementation within a plant simulation, prompting an

estimation of the costs associated with the direct DME synthesis process for an assessment of its actual convenience on an industrial scale.

Author Contributions: Conceptualization, L.M., V.P. and F.F.; methodology, A.D., A.B. and L.M.; software, A.D.; validation, A.D., A.B. and L.M.; formal analysis, A.D.; investigation, S.T., M.S. and C.C.; resources, V.P. and G.B.; data curation, A.D.; writing—original draft preparation, A.D.; writing—review and editing, A.D., A.B., L.M. and G.B.; supervision, G.B.; project administration, V.P.; funding acquisition, G.B. All authors have read and agreed to the published version of the manuscript.

Funding: This research was financially supported by the European Union's Horizon Europe research and innovation program under grant agreement No. 101058540 (project PLASTICE).

Data Availability Statement: Data is contained within the article.

Acknowledgments: The authors also acknowledge Francesco Arena from the University of Messina, Dip. Ingegneria, for the fruitful discussion about the boundary conditions of the kinetic model.

Conflicts of Interest: The authors declare no conflicts of interest.

Appendix A Fugacity Coefficient Evaluation

When working with real mixtures, it is crucial to determine the fugacity coefficient ν_i of each component to measure its deviation from the ideal state. This can be performed by taking advantage of the fact that $\ln \nu_i$ is the partial molar property of $\ln \nu_m$, where ν_m is the fugacity coefficient of the mixture, as described in Equation (A1) [54]:

$$ln\nu_i = ln\nu_m - \sum_{j \neq i} y_j \left(\frac{\partial ln\nu_m}{\partial y_j} \right)_{P,T,y_{k \neq j \neq i}} \tag{A1}$$

In Equation (A1), y_i denotes the molar fraction of compound i, while ν_m was computed through the two-term virial equation of state (Equations (A2)) [55]:

$$ln\nu_m = \frac{B_m P}{RT} \tag{A2}$$

In Equation (A2), P is the reaction pressure, T is the reaction temperature, and R is the universal gas constant, whereas B_m denotes the second virial coefficient of the mixture, which can be evaluated from binary coefficients B_{ij}, as in Equation (A3):

$$B_m = \sum_{i=1}^{7} \sum_{j=1}^{7} y_i y_j B_{ij} \tag{A3}$$

The binary coefficients B_{ij} can be calculated through Tsonopoulos's correlation (Equations (A4)–(A7)), which extends the virial equation to polar fluids [56]:

$$\frac{B_{ij} P_{C_{ij}}}{RT_{C_{ij}}} = f^{(0)}\left(T_{R_{ij}}\right) + \omega_{ij} f^{(1)}\left(T_{R_{ij}}\right) + f^{(2)}\left(T_{R_{ij}}\right) \quad where \quad T_{R_{ij}} = \frac{T}{T_{C_{ij}}} \tag{A4}$$

$$f^{(0)}\left(T_{R_{ij}}\right) = 0.1445 - \frac{0.33}{T_{R_{ij}}} - \frac{0.1385}{T_{R_{ij}}^2} - \frac{0.0121}{T_{R_{ij}}^3} - \frac{0.000607}{T_{R_{ij}}^8} \tag{A5}$$

$$f^{(1)}\left(T_{R_{ij}}\right) = 0.0637 + \frac{0.331}{T_{R_{ij}}^2} - \frac{0.423}{T_{R_{ij}}^3} - \frac{0.008}{T_{R_{ij}}^8} \tag{A6}$$

$$f^{(2)}\left(T_{R_{ij}}\right) = \frac{a_{ij}}{T_{R_{ij}}^6} - \frac{b_{ij}}{T_{R_{ij}}^8} \tag{A7}$$

The terms $f^{(0)}$, $f^{(1)}$ and $f^{(2)}$ represent the impact of intermolecular forces from spherically symmetrical molecules, molecular orientation, and polarity, respectively. All the

critical binary properties figuring in Equation (A4) are evaluated from the critical properties (i.e., critical volume v_C, critical temperature T_C, and critical pressure P_C) and acentric factors ω of pure components, as detailed in Equations (A8)–(A11) [57]:

$$v_{C_{ij}} = \frac{\left(v_{C_i}^{\frac{1}{3}} + v_{C_j}^{\frac{1}{3}}\right)^3}{8} \tag{A8}$$

$$T_{C_{ij}} = \sqrt{T_{C_i} T_{C_j}} \tag{A9}$$

$$P_{C_{ij}} = \frac{T_{C_{ij}}}{2v_{C_{ij}}}\left(\frac{P_{C_i} v_{C_i}}{T_{C_i}} + \frac{P_{C_j} v_{C_j}}{T_{C_j}}\right) \tag{A10}$$

$$\omega_{ij} = \frac{\omega_i + \omega_j}{2} \tag{A11}$$

The a_{ij} and b_{ij} parameters in Equation (A7) measure polar interactions and are exclusively non-zero for pairs of polar fluids. In such instances, they are assumed to be equal to the average of the constants of pure components, as outlined in Equations (A12) and (A13) [55]:

$$a_{ij} = \frac{a_i + a_j}{2} \tag{A12}$$

$$b_{ij} = \frac{b_i + b_j}{2} \tag{A13}$$

In the specific case analyzed, the only polar fluids considered are water, methanol, and dimethyl ether, whose parameters are listed in Table A1.

Table A1. a and b parameters for Equations (A12) and (A13) [55].

Compound	a	b
Water	0.0279	0.0229
Methanol	0.0878	0.0560
Dimethyl Ether	−0.01513	0

Based on the above, in Table A2 are reported the fugacity coefficients as determined under the most severe operating conditions (i.e., 200 °C and 50 bar). The analysis indicates that, in nearly all cases, these coefficients are very close to one, resulting in a negligible correction to the partial pressure. Moreover, although nitrogen shows a measurable deviation from its ideal behavior, its fugacity is not present in the kinetic expressions of the reaction rates (Equations (12)–(14)). Therefore, it was preferred to maintain the validity of the ideal gas hypothesis against a relatively modest enhancement in the model accuracy only achievable behind an increased computational complexity.

Table A2. Fugacity coefficients for different compositions, evaluated at 200 °C and 50 bar.

y_{CO_2}	y_{H_2}	y_{DME}	y_{CO}	y_{Meth}	y_{H_2O}	y_{N_2}	ϕ_{CO_2}	ϕ_{H_2}	ϕ_{DME}	ϕ_{CO}	ϕ_{Meth}	ϕ_{H_2O}	ϕ_{N_2}
0.23	0.69	-	-	-	-	0.08	0.97	1.03	-	-	-	-	0.24
0.21	0.67	-	0.02	-	0.02	0.08	0.97	1.03	-	1.02	-	0.96	0.24
0.21	0.67	0.005	0.007	0.002	0.016	0.09	0.97	1.03	0.98	1.01	0.95	0.96	0.24
0.20	0.63	0.01	0.03	0.01	0.03	0.09	0.97	1.03	0.97	1.01	0.94	0.95	0.24
0.19	0.62	0.02	0.02	0.01	0.06	0.08	0.96	1.04	0.97	1.02	0.93	0.94	0.24

References

1. Fleisch, T.H.; Basu, A.; Gradassi, M.J.; Masin, J.G. Dimethyl Ether: A Fuel for the 21st Century. In *Studies in Surface Science and Catalysis*; Elsevier: Amsterdam, The Netherlands, 1997; pp. 117–125.
2. Matzen, M.; Demirel, Y. Methanol and Dimethyl Ether from Renewable Hydrogen and Carbon Dioxide: Alternative Fuels Production and Life-Cycle Assessment. *J. Clean. Prod.* **2016**, *139*, 1068–1077. [CrossRef]
3. Makoś, P.; Słupek, E.; Sobczak, J.; Zabrocki, D.; Hupka, J.; Rogala, A. Dimethyl Ether (DME) as Potential Environmental Friendly Fuel. *E3S Web Conf.* **2019**, *116*, 00048. [CrossRef]
4. Park, S.H.; Lee, C.S. Applicability of Dimethyl Ether (DME) in a Compression Ignition Engine as an Alternative Fuel. *Energy Convers. Manag.* **2014**, *86*, 848–863. [CrossRef]
5. Park, S.H.; Lee, C.S. Combustion Performance and Emission Reduction Characteristics of Automotive DME Engine System. *Prog. Energy Combust. Sci.* **2013**, *39*, 147–168. [CrossRef]
6. Semelsberger, T.A.; Borup, R.L.; Greene, H.L. Dimethyl Ether (DME) as an Alternative Fuel. *J. Power Sources* **2006**, *156*, 497–511. [CrossRef]
7. Khadzhiev, S.N.; Kolesnichenko, N.V.; Ezhova, N.N. Manufacturing of Lower Olefins from Natural Gas through Methanol and Its Derivatives (Review). *Pet. Chem.* **2008**, *48*, 325–334. [CrossRef]
8. Cordero-Lanzac, T.; Martínez, C.; Aguayo, A.T.; Castaño, P.; Bilbao, J.; Corma, A. Activation of N-Pentane While Prolonging HZSM-5 Catalyst Lifetime during Its Combined Reaction with Methanol or Dimethyl Ether. *Catal. Today* **2022**, *383*, 320–329. [CrossRef]
9. Pérez-Uriarte, P.; Ateka, A.; Aguayo, A.T.; Gayubo, A.G.; Bilbao, J. Kinetic Model for the Reaction of DME to Olefins over a HZSM-5 Zeolite Catalyst. *Chem. Eng. J.* **2016**, *302*, 801–810. [CrossRef]
10. Catizzone, E.; Bonura, G.; Migliori, M.; Frusteri, F.; Giordano, G. CO_2 Recycling to Dimethyl Ether: State-of-the-Art and Perspectives. *Molecules* **2017**, *23*, 31–58. [CrossRef]
11. Bonura, G.; Cordaro, M.; Spadaro, L.; Cannilla, C.; Arena, F.; Frusteri, F. Hybrid Cu–ZnO–ZrO_2/H-ZSM5 System for the Direct Synthesis of DME by CO_2 Hydrogenation. *Appl. Catal. B* **2013**, *140–141*, 16–24. [CrossRef]
12. Wawrzyńczak, D.; Majchrzak-Kuceba, I.; Pevida, C.; Bonura, G.; Nogueira, R.; De Falco, M. *The Carbon Chain in Carbon Dioxide Industrial Utilization Technologies: A Case Study*; Taylor & Francis: Abingdon, UK, 2023.
13. Sankhe, S.; Krishna, S.V.M.; Juturu, R.M.; Subrahmanyam, C. Power-to-X (PtX) Technologies and Their Potential Role in the Transition towards a Fossil-Free Energy Future: A Review of EFuels Synthesis and Direct Air Capture (DAC) Technology. In Proceedings of the International Conference on Automotive Materials and Manufacturing AMM 2023, Pune, India, 1–3 June 2023; SAE Technical Paper 2023-28-1333. pp. 1–5. [CrossRef]
14. Catizzone, E.; Freda, C.; Braccio, G.; Frusteri, F.; Bonura, G. Dimethyl Ether as Circular Hydrogen Carrier: Catalytic Aspects of Hydrogenation/Dehydrogenation Steps. *J. Energy Chem.* **2021**, *58*, 55–77. [CrossRef]
15. Azizi, Z.; Rezaeimanesh, M.; Tohidian, T.; Rahimpour, M.R. Dimethyl Ether: A Review of Technologies and Production Challenges. *Chem. Eng. Process. Process Intensif.* **2014**, *82*, 150–172. [CrossRef]
16. Mondal, U.; Yadav, G.D. Perspective of Dimethyl Ether as Fuel: Part I. Catalysis. *J. CO2 Util.* **2019**, *32*, 299–320. [CrossRef]
17. Bonura, G.; Migliori, M.; Frusteri, L.; Cannilla, C.; Catizzone, E.; Giordano, G.; Frusteri, F. Acidity Control of Zeolite Functionality on Activity and Stability of Hybrid Catalysts during DME Production via CO_2 Hydrogenation. *J. CO2 Util.* **2018**, *24*, 398–406. [CrossRef]
18. Tokay, K.C.; Dogu, T.; Dogu, G. Dimethyl Ether Synthesis over Alumina Based Catalysts. *Chem. Eng. J.* **2012**, *184*, 278–285. [CrossRef]
19. Akhoondi, A.; Osman, A.I.; Alizadeh Eslami, A. Direct Catalytic Production of Dimethyl Ether from CO and CO_2: A Review. *Synth. Sinter.* **2021**, *1*, 105–125. [CrossRef]
20. Chen, W.H.; Hsu, C.L.; Wang, X.D. Thermodynamic Approach and Comparison of Two-Step and Single Step DME (Dimethyl Ether) Syntheses with Carbon Dioxide Utilization. *Energy* **2016**, *109*, 326–340. [CrossRef]
21. Banivaheb, S.; Pitter, S.; Delgado, K.H.; Rubin, M.; Sauer, J.; Dittmeyer, R. Recent Progress in Direct DME Synthesis and Potential of Bifunctional Catalysts. *Chem. Ing. Tech.* **2022**, *94*, 240–255. [CrossRef]
22. Bonura, G.; Cannilla, C.; Frusteri, L.; Catizzone, E.; Todaro, S.; Migliori, M.; Giordano, G.; Frusteri, F. Interaction Effects between CuO-ZnO-ZrO_2 Methanol Phase and Zeolite Surface Affecting Stability of Hybrid Systems during One-Step CO_2 Hydrogenation to DME. *Catal. Today* **2020**, *345*, 175–182. [CrossRef]
23. Ren, S.; Shoemaker, W.R.; Wang, X.; Shang, Z.; Klinghoffer, N.; Li, S.; Yu, M.; He, X.; White, T.A.; Liang, X. Highly Active and Selective Cu-ZnO Based Catalyst for Methanol and Dimethyl Ether Synthesis via CO_2 Hydrogenation. *Fuel* **2019**, *239*, 1125–1133. [CrossRef]
24. Abu-Dahrieh, J.; Rooney, D.; Goguet, A.; Saih, Y. Activity and Deactivation Studies for Direct Dimethyl Ether Synthesis Using CuO–ZnO–Al_2O_3 with NH_4ZSM-5, HZSM-5 or γ-Al_2O_3. *Chem. Eng. J.* **2012**, *203*, 201–211. [CrossRef]
25. Frusteri, L.; Bonura, G.; Cannilla, C.; Todaro, S.; Giordano, G.; Migliori, M.; Frusteri, F. Promoting Direct CO_2 Conversion to DME over Zeolite-Based Hybrid Catalysts. *Pet. Chem.* **2020**, *60*, 508–515. [CrossRef]
26. Ateka, A.; Rodriguez-Vega, P.; Ereña, J.; Aguayo, A.T.; Bilbao, J. Kinetic Modeling and Reactor Design of the Direct Synthesis of Dimethyl Ether for CO_2 Valorization. A Review. *Fuel* **2022**, *327*, 125148. [CrossRef]

27. Hadipour, A.; Sohrabi, M. Synthesis of some bifunctional catalysts and determination of kinetic parameters for direct conversion of syngas to dimethyl ether. *Chem. Eng. J.* **2008**, *137*, 294–301. [CrossRef]
28. Frusteri, F.; Cordaro, M.; Cannilla, C.; Bonura, G. Multifunctionality of Cu–ZnO–ZrO_2/H-ZSM_5 Catalysts for the One-Step CO_2-to-DME Hydrogenation Reaction. *Appl. Catal. B* **2015**, *162*, 57–65. [CrossRef]
29. Delgado Otalvaro, N.; Bilir, P.G.; Herrera Delgado, K.; Pitter, S.; Sauer, J. Kinetics of the Direct DME Synthesis: State of the Art and Comprehensive Comparison of Semi-Mechanistic, Data-Based and Hybrid Modeling Approaches. *Catalysts* **2022**, *12*, 347. [CrossRef]
30. Naik, S.P.; Ryu, T.; Bui, V.; Miller, J.D.; Drinnan, N.B.; Zmierczak, W. Synthesis of DME from CO_2/H_2 Gas Mixture. *Chem. Eng. J.* **2011**, *167*, 362–368. [CrossRef]
31. De Falco, M.; Capocelli, M.; Centi, G. Dimethyl Ether Production from CO_2 Rich Feedstocks in a One-Step Process: Thermodynamic Evaluation and Reactor Simulation. *Chem. Eng. J.* **2016**, *294*, 400–409. [CrossRef]
32. Studt, F.; Behrens, M.; Kunkes, E.L.; Thomas, N.; Zander, S.; Tarasov, A.; Schumann, J.; Frei, E.; Varley, J.B.; Abild-Pedersen, F.; et al. The Mechanism of CO and CO_2 Hydrogenation to Methanol over Cu-Based Catalysts. *ChemCatChem* **2015**, *7*, 1105–1111. [CrossRef]
33. Cao, A.; Wang, Z.; Li, H.; Elnabawy, A.O.; Nørskov, J.K. New Insights on CO and CO_2 Hydrogenation for Methanol Synthesis: The Key Role of Adsorbate-Adsorbate Interactions on Cu and the Highly Active MgO-Cu Interface. *J. Catal.* **2021**, *400*, 325–331. [CrossRef]
34. Campbell, C.T. Finding the Rate-Determining Step in a Mechanism: Comparing DeDonder Relations with the "Degree of Rate Control". *J. Catal.* **2001**, *204*, 520–524. [CrossRef]
35. Lu, W.Z.; Teng, L.H.; Xiao, W. De Simulation and Experiment Study of Dimethyl Ether Synthesis from Syngas in a Fluidized-Bed Reactor. *Chem. Eng. Sci.* **2004**, *59*, 5455–5464. [CrossRef]
36. Li, Z.; Li, N.; Wang, N.; Zhou, B.; Yin, P.; Song, B.; Yu, J.; Yang, Y. Mechanism Investigations on Water Gas Shift Reaction over Cu(111), Cu(100), and Cu(211) Surfaces. *ACS Omega* **2022**, *7*, 3514–3521. [CrossRef] [PubMed]
37. Bonura, G.; Todaro, S.; Frusteri, L.; Majchrzak-Kucęba, I.; Wawrzyńczak, D.; Pászti, Z.; Tálas, E.; Tompos, A.; Ferenc, L.; Solt, H.; et al. Inside the Reaction Mechanism of Direct CO_2 Conversion to DME over Zeolite-Based Hybrid Catalysts. *Appl. Catal. B* **2021**, *294*, 120255. [CrossRef]
38. Motagamwala, A.H.; Dumesic, J.A. Microkinetic Modeling: A Tool for Rational Catalyst Design. *Chem. Rev.* **2021**, *121*, 1049–1076. [CrossRef]
39. Saravanan, K.; Ham, H.; Tsubaki, N.; Bae, J.W. Recent progress for direct synthesis of dimethyl ether from syngas on the heterogeneous bifunctional hybrid catalysts. *Appl. Catal. B Environ.* **2017**, *217*, 494–522. [CrossRef]
40. Din, I.U.; Shaharun, M.S.; Alotaibi, M.A.; Alharthi, A.I.; Naeem, A. Recent Developments on Heterogeneous Catalytic CO_2 Reduction to Methanol. *J. CO2 Util.* **2019**, *34*, 20–33. [CrossRef]
41. Guil-López, R.; Mota, N.; Llorente, J.; Millán, E.; Pawelec, B.; Fierro, J.L.G.; Navarro, R.M. Methanol Synthesis from CO_2: A Review of the Latest Developments in Heterogeneous Catalysis. *Materials* **2019**, *12*, 3902. [CrossRef]
42. Blaszkowski, S.R.; van Santen, R.A. The Mechanism of Dimethyl Ether Formation from Methanol Catalyzed by Zeolitic Protons. *J. Am. Chem. Soc.* **1996**, *118*, 5152–5153. [CrossRef]
43. Jones, A.J.; Iglesia, E. Kinetic, Spectroscopic, and Theoretical Assessment of Associative and Dissociative Methanol Dehydration Routes in Zeolites. *Angew. Chem.* **2014**, *126*, 12373–12377. [CrossRef]
44. Ghorbanpour, A.; Rimer, J.D.; Grabow, L.C. Computational Assessment of the Dominant Factors Governing the Mechanism of Methanol Dehydration over H-ZSM-5 with Heterogeneous Aluminum Distribution. *ACS Catal.* **2016**, *6*, 2287–2298. [CrossRef]
45. Tang, Q.-L.; Liu, Z.-P. Identification of the Active Cu Phase in the Water−Gas Shift Reaction over Cu/ZrO_2 from First Principles. *J. Phys. Chem. C* **2010**, *114*, 8423–8430. [CrossRef]
46. Madon, R.J.; Braden, D.; Kandoi, S.; Nagel, P.; Mavrikakis, M.; Dumesic, J.A. Microkinetic Analysis and Mechanism of the Water Gas Shift Reaction over Copper Catalysts. *J. Catal.* **2011**, *281*, 1–11. [CrossRef]
47. Lacerda de Oliveira Campos, B.; Herrera Delgado, K.; Wild, S.; Studt, F.; Pitter, S.; Sauer, J. Surface Reaction Kinetics of the Methanol Synthesis and the Water Gas Shift Reaction on Cu/ZnO/Al_2O_3. *React. Chem. Eng.* **2021**, *6*, 868–887. [CrossRef]
48. Behloul, C.R.; Commenge, J.-M.; Castel, C. Simulation of Reactors under Different Thermal Regimes and Study of the Internal Diffusional Limitation in a Fixed-Bed Reactor for the Direct Synthesis of Dimethyl Ether from a CO_2-Rich Input Mixture and H_2. *Ind. Eng. Chem. Res.* **2021**, *60*, 1602–1623. [CrossRef]
49. Agarwal, A.K.; Brisk, M.L. Sequential Experimental Design for Precise Parameter Estimation. 1. Use of Reparameterization. *Ind. Eng. Chem. Process Des. Dev.* **1985**, *24*, 203–207. [CrossRef]
50. Pritchard, D.J.; Bacon, D.W. Statistical Assessment of Chemical Kinetic Models. *Chem. Eng. Sci.* **1975**, *30*, 567–574. [CrossRef]
51. Espie, D.M.; Macchietto, S. Nonlinear Transformations for Parameter Estimation. *Ind. Eng. Chem. Res.* **1988**, *27*, 2175–2179. [CrossRef]
52. Ereña, J.; Sierra, I.; Aguayo, A.T.; Ateka, A.; Olazar, M.; Bilbao, J. Kinetic Modelling of Dimethyl Ether Synthesis from (H_2 + CO_2) by Considering Catalyst Deactivation. *Chem. Eng. J.* **2011**, *174*, 660–667. [CrossRef]
53. Ahmad, K.; Upadhyayula, S. Greenhouse Gas CO_2 Hydrogenation to Fuels: A Thermodynamic Analysis. *Environ. Prog. Sustain. Energy* **2019**, *38*, 98–111. [CrossRef]
54. Marrelli, L. *Termodinamica Degli Equilibri Di Fasi Fluide*; Edizioni Efesto: Rome, Italy, 2017.

55. De Santis, R. *Introduzione al Calcolo Degli Equilibri Di Fasi Fluide*; ESA: Paris, France, 1991.
56. Tsonopoulos, C. An Empirical Correlation of Second Virial Coefficients. *AIChE J.* **1974**, *20*, 263–272. [CrossRef]
57. Chueh, P.L.; Prausnitz, J.M. Vapor-Liquid Equilibria at High Pressures. Vapor-Phase Fugacity Coefficients in Nonpolar and Quantum-Gas Mixtures. *Ind. Eng. Chem. Fundam.* **1967**, *6*, 492–498. [CrossRef]